J. Sustain. Metall. (2016) 2:405–415
DOI 10.1007/s40831-016-0062-8

RESEARCH ARTICLE

Sustainable Electrochemical Synthesis of Large Grain- or Catalyst-Sized Iron

Fang-Fang Li[1] · Baohui Wang[1] · Stuart Licht[1]

Published online: 2 June 2016

Abstract Electrolytic production of iron in molten salts by splitting iron oxide into iron metal and O_2 is a low-carbon footprint alternative to the massive CO_2 emissions associated with conventional carbothermal iron production and permits. This study advances a CO_2-free method for iron production, by modifying iron electrosynthesis in molten Li_2CO_3 to control iron product particle size and by decreasing the electrolyte extracted with the pure iron product. We present the first study of electrolytic iron micro-morphology as formed from iron, and demonstrate it is strongly influenced by the deposition conditions. Particle size and morphology are critical characteristics in a variety of metal applications. In this study, large ($\sim$500 μm) iron particles are formed at low current densities during extended electrolysis, or at high Fe(III) concentrations, and small ($\sim$10 μm) at high current density and low Fe(III). Deposited Fe is fiber shaped from equal molals of Fe_2O_3 and Li_2O, but particle-like from electrolytes with surplus Li_2O. Iron is formed at high current efficiency, and the observed electrolysis potential decreases with (i) the decreasing current density, (ii) addition of Li_2O, (iii) the increasing anode area, and (iv) the increasing temperature.

Keywords Iron production · Carbon dioxide mitigation · Molten carbonate · Iron electrochemistry

✉ Stuart Licht
slicht@gwu.edu

[1] Department of Chemistry, George Washington University, Washington, DC 20052, USA

Introduction

The prevalent form of iron oxide used for iron production is hematite, Fe_2O_3. Iron and steel manufacturing is the largest industrial source of greenhouse gases contributing 7 % of the total world's emissions from human activities [1]. In the iron smelting process, metallic iron is formed via carbon reduction at high temperature in accordance with the reaction:

$$Fe_2O_3 + 3/2C \rightarrow 2Fe + 3/2CO_2 \quad (1)$$

The Fe_2O_3 reduction reaction, Eq. 1, is endothermic, requiring the heat of burning additional carbon, and releasing additional carbon dioxide in addition to that generated in Eq. 1, exacerbating the carbon dioxide pollution due to conventional iron production. Iron and oxygen can be formed by electrolysis in molten iron oxide, but that process is constrained by material challenges of the very high melting point of iron oxide (1550 °C) [2, 3]. Iron oxides (both hematite, as well as another common iron oxide, magnetite, Fe_3O_4) while insoluble in sodium or potassium carbonates become highly soluble (containing up to 50 % by weight iron oxide) in lithiated molten carbonates [4–7]. The melting point of the Li,Na,K carbonate eutectic is 399 °C and that of pure Li_2CO_3 is 723 °C, and both can dissolve high concentrations of iron oxide. This solubility is observed as the soluble salt $LiFeO_2$ which is formed in combination with Li_2O [6]:

$$Fe_2O_3 + Li_2O(\text{soluble}) \rightarrow 2LiFeO_2(\text{soluble in molten } Li_2CO_3) \quad (2)$$

The high iron oxide solubility in molten carbonate suggests a non-CO_2-emitting electrolytic process for the production of iron in which iron ore (as Fe_2O_3 or Fe_3O_4)[5] dissolves in molten carbonate at $\sim$750 °C) and is split by

electrolysis at low voltage and high current efficiency into iron metal and oxygen without carbon dioxide emission [5].

No carbon dioxide is emitted when the heat for this electrolytic production of iron metal is provided by solar energy converted to thermal energy, and the electrolysis current is provided by solar or other renewable energy converted to electronic energy. The splitting of Fe_2O_3 into Fe(metal) and O_2 is endothermic, and the thermodynamic electrolysis potential (1.28 V at 25 °C) falls with the increasing temperature. The general solar thermal electrochemical process (STEP) of sunlight to decrease (endogenic) electrolysis potentials leads to high solar energy conversion efficiencies [6–11]. A variety of other STEP electrolyses have been demonstrated to decrease CO_2 including the production of cement, ammonia, fuels, and carbon for the direct removal of atmospheric or smokestack carbon dioxide [10–20]. Fundamental, electrochemical, and impurity effects on STEP iron have been investigated [8], and the general effects of alkali earth and hydroxide on STEP processes in molten carbonates have been reported [14–20]. The fundamental increase in solar electrolysis efficiency with the use of solar thermal has been analyzed for CO_2 and H_2O splitting theoretically [10–12] and experimentally [13–15] and the fundamental endogenic decrease in electrochemical potential with the increasing temperature demonstrated for a number of STEP processes [10–20]. The requisite solar thermal heating for any given process will depend on the current density, which controls the overpotential and the net difference between the thermoneutral potential and the applied electrolysis potential.

We have previously delineated the solar, optical, and electronic components of STEP iron [5–8]. In this study, we focus on the electrolysis component of STEP iron. Specifically, we present the first study of the micro-morphology of STEP iron products, as well as the in-process removal of the electrolyte from the deposited metal iron product. We demonstrated the high purity of the iron product obtained [7], but did not study the micro-morphology of this iron. Particle size and morphology are critical characteristics in a variety of metal and metal oxide applications including catalysis, epoxy composites, MRI, drug delivery, magnetic separation, and immobilization of biosubstances [21–23]. In catalytic reactions, the size of the catalyst is one of the factors to affect its catalytic efficiency [24, 25]. For example, as the catalyst for STEP ammonia synthesis in our previous studies, the iron particle size is critical for its performance [26]. Large iron particles did not catalyze the reaction effectively, while small particles on the order of several microns react with nitrogen and water to form ammonia in molten salts at high rate.

Electrolytic production of iron in molten salts by splitting iron oxide into iron metal and O_2 is a low-carbon footprint alternative to the massive CO_2 emissions associated with conventional carbothermal iron production and as shown here permits new morphological control over the product. Here, we present the first study of electrolytic iron micro-morphology as formed from iron oxide in molten Li_2CO_3. We demonstrate that the electrolytic iron micro-morphology product is strongly influenced by the deposition conditions, including the iron particle shape and a two-order of magnitude variation of iron product particle size. This study advances a CO_2-free production method for iron modifying the synthesis to control iron product particle size and by decreasing the electrolyte extracted with the pure iron product.

Experimental

Chemicals and Materials

Lithium carbonate (Alfa Aesar, 99 %), lithium oxide (Alfa Aesar, 99.5 %), lithium hydroxide (Acros Organics, 98 %), barium carbonate (Alfa Aesar, 99.5 %), and calcium carbonate (Alfa Aesar, 98 %) are combined to form various molten electrolytes. Ferric oxide (Fe_2O_3) (Alfa Aesar, 98 %) was added to the molten electrolytes.

Electrolysis

Electrolysis are driven galvanostatically at a fixed current as described in the text. The electrolysis is contained in a high purity alumina crucible (99.6 %, AdValue Technology AL-2100) or Ni crucible (VWR AA35906-KY). Electrolysis used coiled Ni wire (Alfa Aesar, 99.5 %) as the (oxygen generating) anode. A wide variety of iron and steel wires for coiled cathodes are effective, an economic form (used in this study) is Fi-Shock 14 Gauge, Steel Wire model #BWC-14200. The electrolysis potential is measured as the voltage between the anode and the cathode at constant current. We have previously reported on STEP cathode or oxygen anode potentials in a variety of molten carbonates [5–20] During electrolysis, the iron product accumulates at the cathode, which is subsequently removed and cooled. Details of STEP electrolysis are provided in references [5–8].

Characterization

The iron product is washed, and analyzed titrametrically and by PHENOM Pro-X Energy Dispersive Spectroscopy on the PHENOM Pro-X Scanning Electron Microscope. Magnification size bars are indicated on the Scanning Electron Microscopy images, SEM. The procedure for determining total metallic iron in the cathode product is

(1) The cathode product is ground in mortar and pestle, until it can be sifted and dispersed through a 70-mesh (212 μm) sieve.

(2) The ground product is washed with deionized water, and then extracted by vacuum filtration and rinsing the precipitate with deionized water until pH is near 7. The precipitates, residue, and filter paper are collected to react with $CuSO_4$.

(3) To 0.5 g of the ground product is added 50 ml of 0.5 M $CuSO_4$, to form

$$Fe + CuSO_4 \rightarrow FeSO_4 + Cu \quad (3)$$

(4) After boiling this slowly stirred solution for 1 h, it is immediately filtered (to prevent the reaction of O_2 with Fe^{2+}) with a GF/A (Whatman glass microfiber) filter paper into a 250 ml volumetric flask, and the filter paper is washed with double deionized (18 MΩ) water also into the flask, and diluted to 250 ml. The iron analysis reliability improves with slow, instead of fast, stirring (an underestimate of the Fe^0 content of the product occurs with the increasing speed of stirring) due to the introduction of oxygen, which can convert ferrous to ferric prior to the titration.

(5) 25 ml of the 250 ml filtrate is sampled by pipette into a 250-ml Erlenmeyer flask, and the following solutions are added to the flask: 20 ml of "A", 20 ml of "B", 50 ml of water, and 3 drops of indicator solution "C", where A: a mix of 50 ml of water with 10 ml concentrated H_2SO_4; B: 700 ml of water with 150 ml concentrated H_2SO_4, 150 ml H_3PO_4 (binds colored Fe^{3+}, which is colored, as colorless $Fe(HPO_4)_2^-$, to improve clarity of the endpoint); C: the indicator solution consisting of 0.2 % aqueous Diphenlyamine 4-sulfonic acid sodium salt; D: the titrant consisting of 0.004167 M (6 × dilution of 0.025 M) $K_2Cr_2O_7$ which titrates as 1 equivalent $K_2Cr_2O_7$ per $FeSO_4$; for each ml of solution, D = 1.3962 mg of Fe° metal.

$$6FeSO_4 + K_2Cr_2O_7 + H_2SO_4 \rightarrow 3Fe_2(SO_4)_3 + K_2SO_4 + Cr_2(SO_4)_3 + 7H_2O \quad (4)$$

The endpoint is observed as a color change from light blue (initial) to the endpoint's purple.

This titration analysis is also confirmed by weighing the mass of magnetically removed the iron product that was washed & dried to remove oxide. The need to switch to a lower stirring speed for the Fe^0 analysis was discovered and applied to the latter half of the experiments in this study. Under this latter condition replicate analyses of Fe^0 metal mass from are reproducible to within a ±2 %.

Results and Discussion

The melting point of lithium carbonate, Li_2CO_3, is 723 °C. This melting point decreases with the increasing concentrations of added salts [7]. The high iron oxide solubility in molten lithium carbonate led us to a non-CO_2 emitting electrolytic process for the production of iron:

$$2LiFeO_2(\text{soluble}) \rightarrow 2Fe + Li_2O\ (\text{soluble}) + 3/2O_2 \quad (5)$$

Lithium oxide liberated during the electrolysis Eq. 5 allows for the continuous addition and dissolution of iron oxide in Eq. 2. Hence, iron is formed by the continuous addition of Fe_2O_3 (the principle constituent of iron ore) without the need to add additional lithium oxide. This iron oxide splitting electrolysis mechanism has been delineated in references 5-8, and the minimum electrolysis potential for a related process (for splitting carbon dioxide by electrolysis in molten carbonate) has also been investigated [9]. Instead of the carbothermal production of iron, Eq. 1, the net process for the electrolytic formation of iron metal via the sum of Eqs. 2 and 5 is given by [6]

$$Fe_2O_3 \rightarrow 2Fe + 3/2O_2 \quad (6)$$

In the absence of dissolved iron oxide, rather than

$$\begin{aligned} &\text{Dissolution}: Fe_2O_3 + Li_2O(\text{soluble}) \\ &\qquad \rightarrow 2LiFeO_2(\text{soluble in molten } Li_2CO_3) \\ &\text{Electrolysis}: 2LiFeO_2(\text{soluble}) \rightarrow 2Fe \\ &\qquad + Li_2O\ (\text{soluble}) + 3/2O_2 \\ &\text{Net}: Fe_2O_3 \rightarrow 2Fe + 3/2O_2 \end{aligned} \quad (7)$$

Dissolution of carbon dioxide and splitting of the electrolyte lead to carbon formation at $T < 900$ °C:

$$\begin{aligned} &\text{Dissolution}: CO_2 + Li_2O(\text{soluble}) \rightarrow Li_2CO_3 \\ &\text{Electrolysis}: Li_2CO_3 \rightarrow C + Li_2O\ (\text{soluble}) + O_2 \\ &\text{Net}: CO_2 \rightarrow C + 1O_2 \end{aligned} \quad (8)$$

and with the increasing temperature shifts to a carbon monoxide product at $T > 900$ °C:

$$\begin{aligned} &\text{Dissolution}: CO_2 + Li_2O(\text{soluble}) \rightarrow Li_2CO_3 \\ &\text{Electrolysis}: Li_2CO_3 \rightarrow CO + Li_2O\ (\text{soluble}) + O_2 \\ &\text{Net}: CO_2 \rightarrow CO + 1/2O_2 \end{aligned} \quad (9)$$

The individual anode and cathode reactions can be complex [7–9], but in all cases, O_2 is generated at the anode and the reduced carbon or iron product at the cathode.

Figure 1 presents the observed variation of the iron oxide splitting electrolysis potential at 730 °C with the increasing current during electrolysis in a Li_2CO_3 electrolyte containing 3mLi_2O and 1.5 m Fe_2O_3 (m = molal, moles per kg Li_2CO_3). In each case, the electrolysis was conducted for 1 Ah at a 10 cm^2 nickel anode and a 10 cm iron cathode (10 h for the 0.1 A electrolysis, decreasing to 0.2 h for the 5 A electrolysis). The expected increase of potential with current density is evident. Not shown is that the electrolysis potential is smaller than the low value of 1.2 V in the figure for the 0.1 A electrolysis, and is less than 1 V when the electrolysis is conducted either at higher temperature, or with a larger anode to diminish the substantial anode O_2 evolution polarization contribution to the overpotential [8].

Cross-sectional analysis of the iron in cathode deposit shows that the top layer (nearest the anode) is dominated by Fe(III), the middle layer by Fe(II,III), and the bottom layer on the cathode by Fe(0). The electrolyte resistance impacts the electrolysis potential at higher current density. The electrolysis potential for the 5 A electrolysis in Fig. 1 decreases by up to 0.8 V when the anode/cathode spacing is diminished (not shown), but is not observably smaller for the 0.1 A electrolysis. However, when the inter electrode spacing is closer than that shown in the photo, there is a tendency that an electrical short occurs as the iron metal product grows from the cathode and contacts the anode during extended (high Q, total charge) electrolysis.

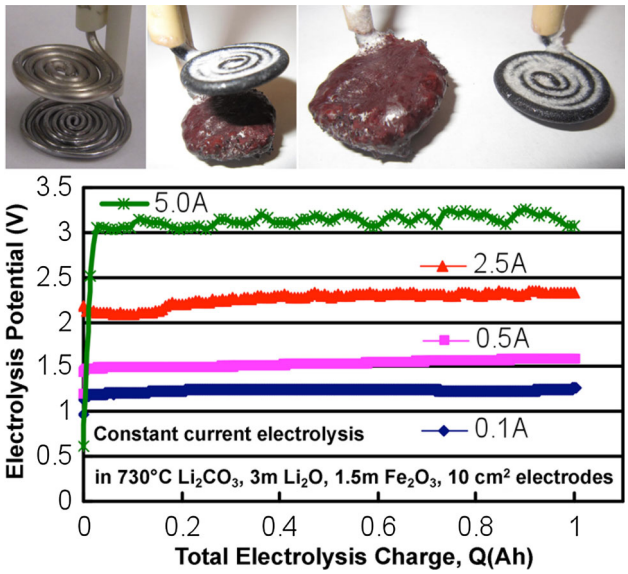

Fig. 1 Variation of the iron oxide splitting electrolysis potential with currents for a fixed (1 Ah) total charge. The electrolysis was conducted in 730 °C Li_2CO_3 with 3 m Li_2O and 1.5 m Fe_2O_3 for 1 Ah at a 10 cm^2 nickel anode and a 10 cm^2 iron cathode. Photos: 10 cm^2 nickel anode above a 10 cm^2 iron cathode before (*left photo*) immersion in the electrolyte and after the electrolysis (*middle* and *right photos*). Post-electrolysis cathode product is removed, washed, and analyzed for iron metal. The iron wire is re-useable as a cathode

An unexpectedly large effect of current density on iron product particle size formed by electrolysis from molten carbonate is seen by comparison of the SEM in Fig. 2. All of the SEM observations are presented at the same magnification. Although each electrolysis is conducted for 1 Amp hour (Ah) of charge, the iron particle size formed varies by an order of magnitude with current density. In each case, the electrolysis is conducted in 730 °C molten lithium carbonate containing 3 m Li_2O and 1.5 m Fe_2O_3 charge through an oxygen generating 10 cm^2 nickel anode and an iron forming 10 cm^2 iron cathode. As shown in Fig. 1, product iron was formed at four different current densities, (A) 10 mA cm^{-2} (0.1 A electrolysis for 10 h, to cm^{-2} (2.5A for 0.4 h), or (D) 500 mA cm^{-2} (5 A for 0.2 h). The figure demonstrates that the size of deposited Fe varies inversely with current at a fixed charge, varying from 100 to 300 μm at a low current density of 10 mA cm^{-2}, down to 10–30 μm at high current density of 500 mA cm^{-2} for these 1 Ah electrolysis. It is speculated that diffusional (mass transport) limitations imposed by higher current density preferentially support repeated nucleation and growth of new iron particles, rather than ongoing growth of existing iron particles.

In addition to the study of the systematic variation of the iron product micromorphology with current density, oxide concentration, electrolysis temperature, electrolysis time, iron concentration, and electrolysis charge were studied as well (Figs. 2, 4, 5, 6, 7, and 8), which can occur with change in conditions, in this case a change of electrolyte. LiOH was added to introduce a potential source of bound water in the electrolyte to encourage the possibility of an iron oxide particle formation with the iron product. The use of a mixed cation electrolyte lowers the melting point to encourage some (bound) water retention in the electrolyte. Figure 3 presents SEM of the substantial morphology variation of the iron product that can form during electrolysis under these significantly different electrolysis conditions in molten carbonate. This product was formed at longer electrolysis time (2 h compared to 0.4 h at 2.5 A previously), lower temperature (650 °C compared to 730 °C), and in a different electrolyte of $Li_{1.34}Ba_{0.08}Ca_{0.1}CO_3$ with 6 m LiOH and 1.5 m Fe_2O_3.

The product particle size formed during a 250 mA cm^{-2} electrolysis shown in Fig. 3 is similar in size to that formed in the Li_2CO_3 electrolyte in Fig. 2 at 2.5 A the same current density, but the product appears more granular. In Fig. 3, this single iron product is shown at magnifications increasing from ×270 (top left) to ×14500 in bottom right. Unlike the previous higher-temperature electrolyte, which contained Li_2O, this electrolyte contains LiOH, which

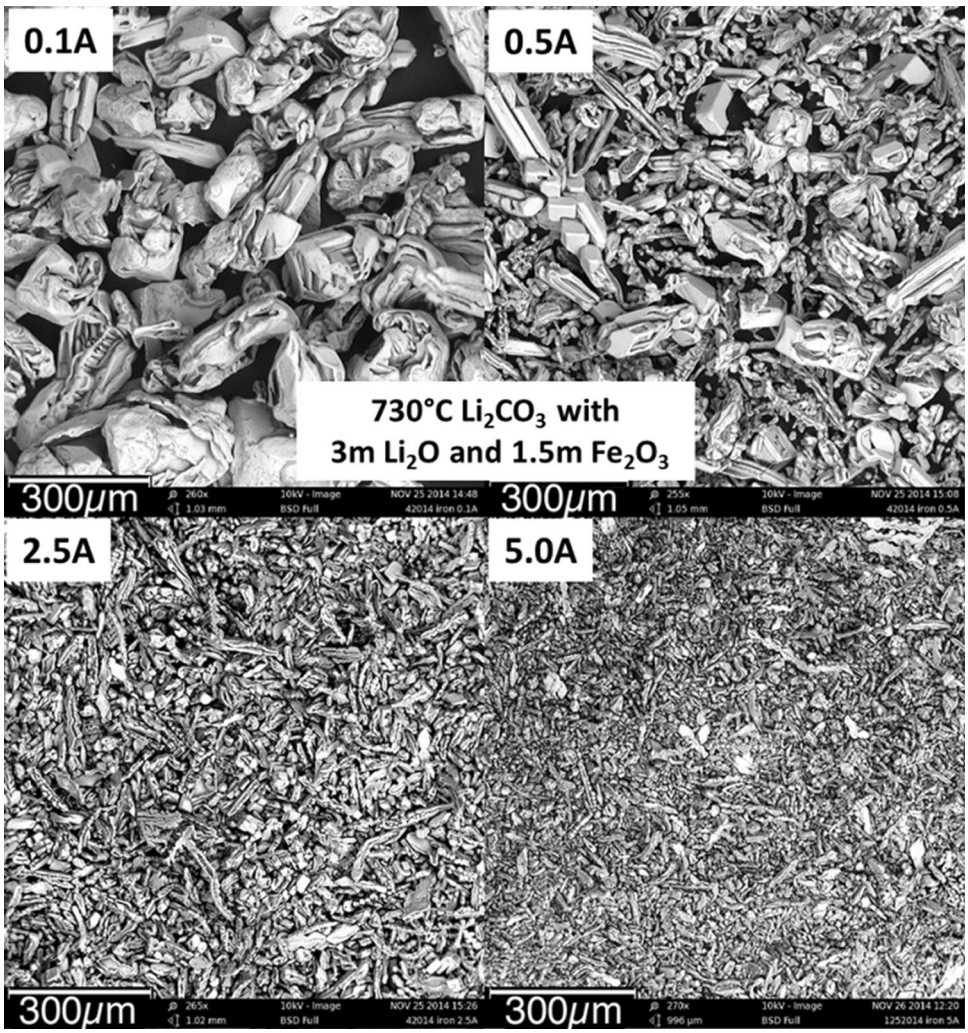

Fig. 2 SEM of the iron metal product formed at different electrolysis current densities in identical electrolytes and with the same electrolysis charge (1 Ah). The electrolyte is 730 °C Li_2CO_3 with 3 m Li_2O and 1.5 m Fe_2O_3. Iron is formed by electrolytic splitting of iron oxide in carbonate at the indicated currents of 0.1, 0.5, 2.5, or 5 A. The electrolysis was conducted at a 10 cm^2 nickel anode and a 10 cm^2 iron cathode. Post-electrolysis cathode product is removed and washed

allows water to be available in accordance with the equilibrium:

$$2LiOH \rightleftharpoons Li_2O + H_2O \quad (10)$$

It is seen in Fig. 3 that the iron product is strongly affected by the electrolyte deposition conditions. In particular, the available water induces an overlayer of Fe_3O_4 (as determined by EDS analysis of the sample, and the known octahedral crystal shape of magnetite).

Figure 4 presents the effect of Li_2O concentration in a 730 °C molten Li_2CO_3 electrolyte containing 1.5 m Fe_2O_3, on the morphology of the cathode electrolysis product; specifically with either 1.5 m Li_2O (left side of the figure), 3 m Li_2O (middle) or 9 m Li_2O (right). The 1 Ah electrolysis are conducted at either low (0.1 A—top row of the figure) or high 5 A (bottom row) constant current. In accordance with Eq. 2, the electrolytes are composed of dissolved 3 m $LiFeO_2$ either without surplus Li_2O (left side), or with 1.5 m (middle) or 7.5 m (right) surplus Li_2O. At 0.1 A, the low oxide electrolyte generates 3-fold longer ($\sim$600 μm length) iron particles (top, left). For the 5 A electrolysis, the production of longer iron particles is also evident from the low oxide electrolyte (bottom, left). Li_2O concentrations have also been observed to effect the morphology of carbon nanotubes and nanofibers grown from molten Li_2CO_3 (in the absence of added iron oxide), and specifically that higher Li_2O concentrations lead to the growth of tangled, rather than straight nanostructures [27, 28].

Variation of lithium oxide concentration in the molten carbonate electrolyte has several effects on the iron oxide electrolysis in addition to the product morphology as observed in Fig. 4. Consistent with prior observations, the electrolysis potential decreases with the increasing Li_2O concentration [8]. For example, in the 5 A constant current electrolysis at 730 °C in the 3 m Li_2O, the average potential is 3.1 V, but we observe that a higher 3.4 V during the 1.5 m Li_2O electrolysis, and a lower 2.9 V average electrolysis in the 9 m Li_2O electrolyte.

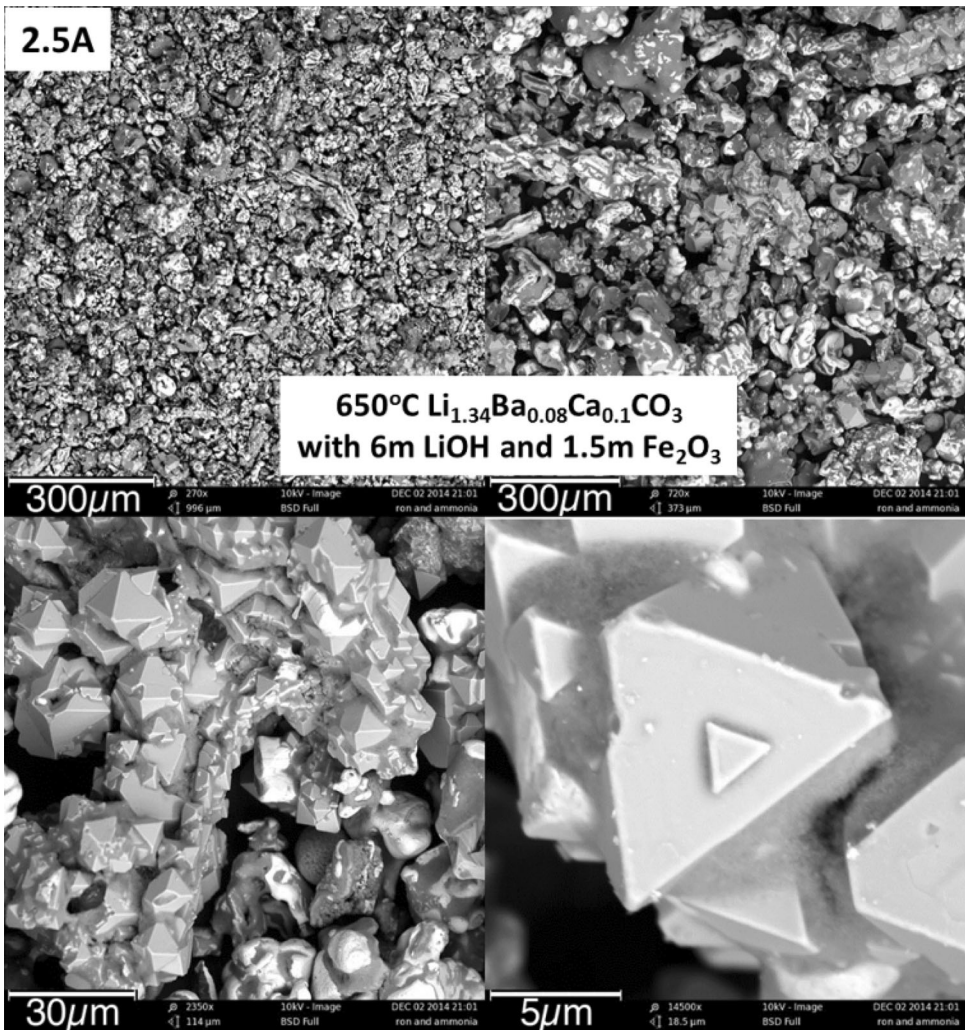

Fig. 3 Variation of the iron product shape with a substantial change in electrolysis conditions. The 1.5 m Fe_2O_3 electrolysis is conducted in 650 °C $Li_{1.34}Ba_{0.08}Ca_{0.1}CO_3$ with 6 m LiOH compared to 730 °C Li_2CO_3 with 3 m Li_2O in Fig. 2. Electrodes are as described in the Fig. 2 caption, and the current is the same as in the 2.5 A Fig. 2, but is applied for 2 h (5 Ah). Both the deposited iron and the formation of a product of octahedral magnetite, Fe_3O_4 are observed

According to Eq. 6, one equivalent of metallic iron can be formed with three equivalents of applied charge. The iron electrolysis columbic efficiency is defined as 100 % × the measured moles of iron product divided by 3 × the measured equivalents of charge passed during the electrolysis (1 Ah = 3600 coulombs = 0.037 Faraday of electrons). Generally, STEP iron coulombic efficiency approaches 100 % [7]. Any losses from this 100 % coulombic efficiency can be attributed to (i) the partial reduction to Fe_3O_4, rather than to iron metal, visible as a mixed black (magnetite) product in the outer perimeter of the cathode product and by chemical analysis [7]; (ii) nickel deposited at the cathode as a consequence of anodic corrosion; (iii) chemical re-oxidation of the iron metal product by high oxide concentrations; or (iv) the co-deposition of reduced carbon in the iron which is only observed to occur at higher potentials than for iron deposition [6, 11]. We have previously detailed the thin oxide layer that develops on the nickel anode, and that is highly stable toward O_2 formation in molten Li_2CO_3 containing up to 5 m Li_2O [8]. Higher Li_2O concentrations lead to corrosion of the anode and release of low concentrations of oxidized nickel into the electrolyte. The majority of the applied current yields iron metal during electrolysis in either low or moderate Li_2O-containing electrolytes (left and middle of Fig. 4). However, in the high oxide electrolyte prepared with 9 m Li_2O, corrosion of the anode is visible, and the iron formed is measured at 6 % columbic efficiency.

Elevated temperature can decrease the electrolysis potential and power required for iron deposition. At 950 °C, rather than 730 °C, the average electrolysis potential drops from 3.1 V to 1.9 V at 5A in the 3 m Li_2O, 1.5 m Fe_2O_3 lithium carbonate electrolyte, and drops from 1.2 V down to 0.6 to 0.8 V at 0.1 A. Interestingly as seen in Fig. 5, at 950 °C the product particle size from the 5 A electrolysis is larger than that observed for the 730 °C electrolysis product seen in Fig. 2.

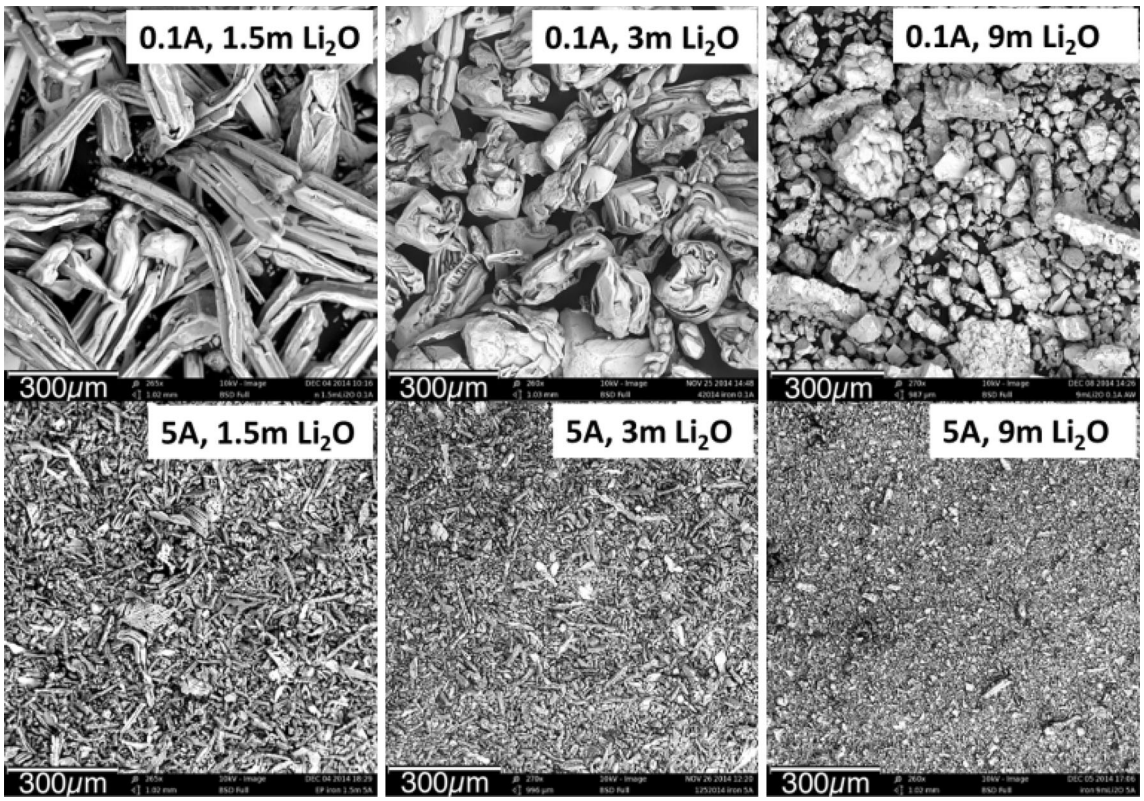

Fig. 4 SEM of the cathode product formed in molten lithium carbonate with various, increasing concentrations of Li_2O. The electrolyte is 730 °C Li_2CO_3 with 1.5 m Fe_2O_3 and with the indicated 1.5, 3, or 9 m concentration of Li_2O. Iron is formed by a 1 Ah electrolysis between a 10 cm^2 Ni anode and a 10 cm^2 iron cathode at the indicated current (either 0.1 or 5 A). Expanded copies of the middle SEM are seen in Figs. 2a, d

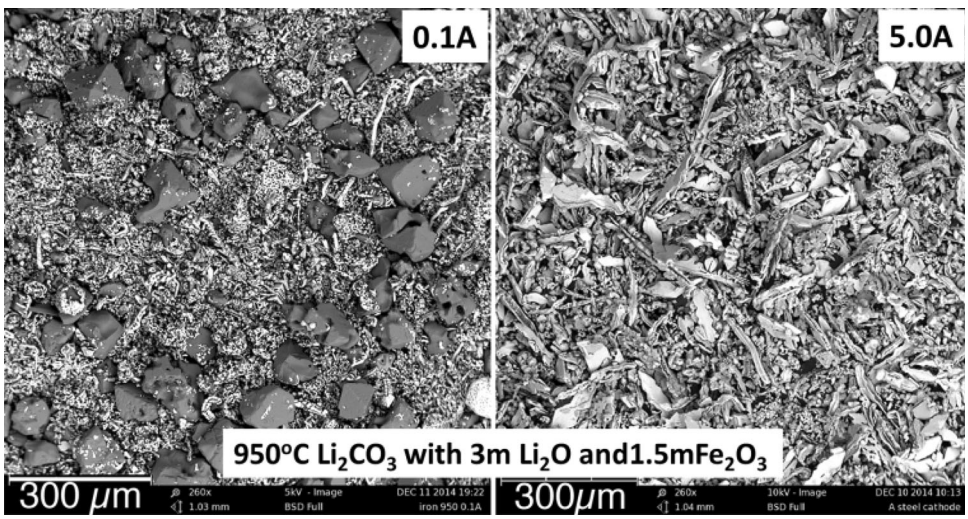

Fig. 5 SEM of the product formed by elevated temperature, 1 Ah electrolysis at 950 °C in Li_2CO_3 with 3 m Li_2O and 1.5 m Fe_2O_3. Electrolysis is driven at the indicated 0.1 A or 5 A current. Electrodes are as described in the Fig. 2 caption

Assuming constant coulombic efficiency and density at constant current, toward a linear increase in volume, the diameter of the iron product particles would be expected to increase linearly with the cube root of the relative increase in deposition time. As compared in Figs. 2 and 6, by shortening the electrolysis time at constant current, the iron

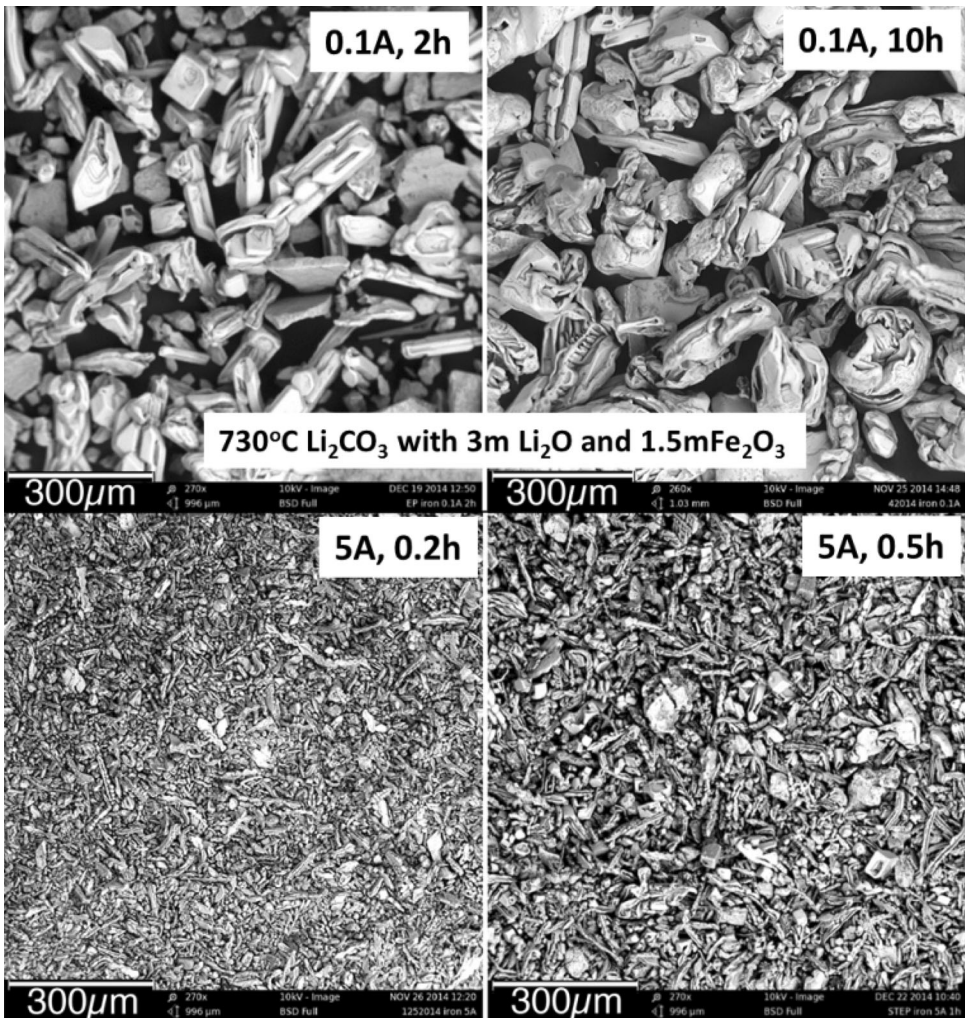

Fig. 6 SEM of Fe variation with electrolysis time. Electrolysis conducted at 0.1 A (*top*) as indicated for either 2 h (total charge 0.2 Ah) or 10 h (total charge 1 Ah), or at 5A (*bottom*) as indicated for 0.2 h (total charge 1 Ah) or 0.5 h (total charge 2.5 Ah)

product particle size is smaller, and in turn it becomes larger by prolonging the electrolysis time in the 730 °C Li_2CO_3 with 3 m Li_2O and 1.5 m Fe_2O_3 electrolyte.

No significant effect on iron product particle size was observed when the iron oxide was electrolyzed in molten lithium carbonate under CO_2 gas, rather than under nitrogen gas. Similarly, the use of an oversized anode did not significantly alter the iron particle size. Specifically, the alumina crucible was replaced by a nickel crucible, and the 10 cm^2 wound nickel wire anode was replaced by the inner walls of the nickel crucible. The cathode product from this electrolysis conducted in 730 °C Li_2CO_3, 3 mLi_2O, 1.5 m Fe_2O_3 at 0.1A for 10 h was similar to the product shown in Fig. 2a, although the electrolysis occurred at a lower average potential of 0.98 V due to the larger anode surface area.

Figure 7 compares the iron variation with $LiFeO_2$ concentration in the 730 °C lithium carbonate electrolytes. In each case, in accordance with Eq. 2, the $LiFeO_2$ concentration is prepared by dissolution of equal concentrations of ½ Fe_2O_3 + ½ Li_2O. Previously in molten Li_2CO_3, cyclic voltammetry has observed a single peak related to the reduction of Fe(III) for dissolved Fe_2O_3, and two peaks related the reduction of Fe(II) and Fe(III) for dissolved Fe_3O_4 [5]. The concentrations of Fe(III), dissolved as $LiFeO_2$, significantly impact the electrolysis product in molten carbonates. In the absence of Fe(III) added to the electrolyte, the cathode product from molten lithium carbonate is either pure solid carbon (at temperatures at or below 750 °C) or a mix of carbon and carbon monoxide gas at temperatures up to 900 °C, or carbon monoxide at temperature of 950 °C instead of an iron metal cathode product. At low concentration of Fe(III), such as 0.2 m $LiFeO_2$ (formed by the dissolution of 0.1 m Li_2O and 0.1 m Fe_2O_3 in Li_2CO_3 at 730 °C), the cathode product is a mix of iron and solid carbon. This occurs even at a low current density of 10 mA cm^{-2}, and the product particle size is small as seen in the left and middle top portions of

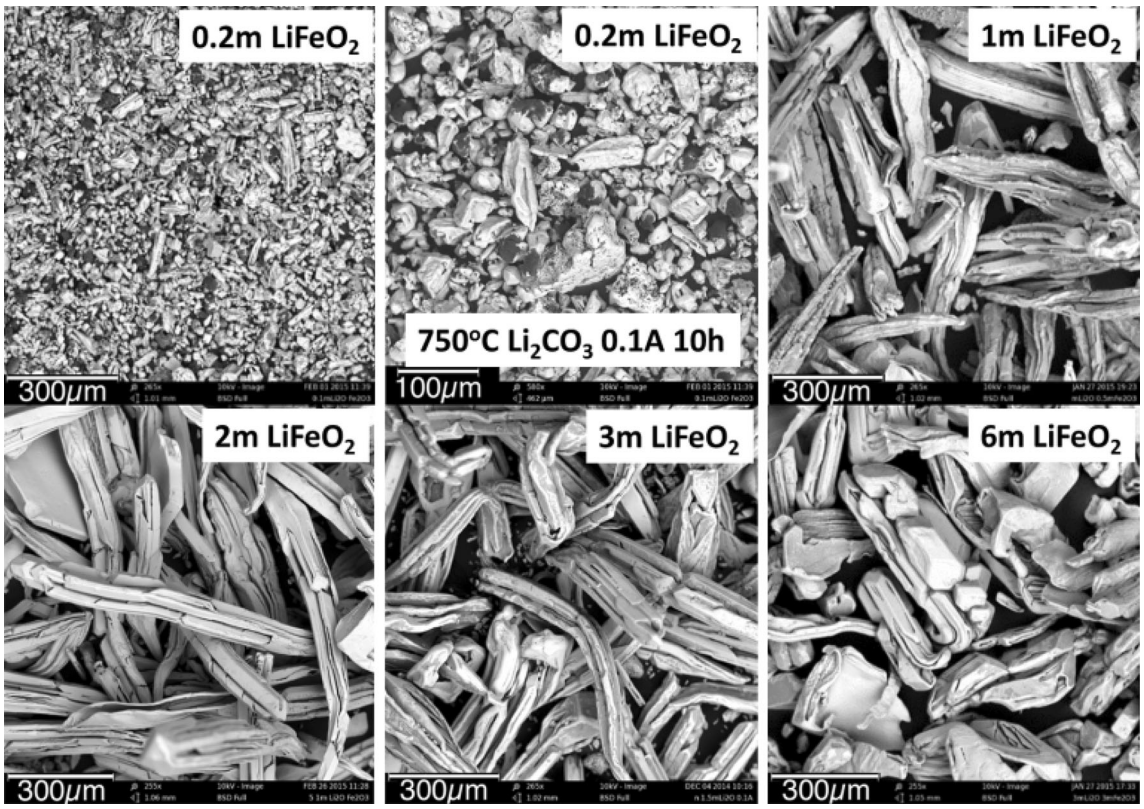

Fig. 7 Fe variation with $LiFeO_2$ concentrations (Li_2CO_3 electrolytes with equimolal Li_2O and Fe_2O_3). Iron formed at 0.1A for 10 h (1 Ah of charge). In the *top left* and *middle panels*, the electrolysis was conducted with 0.2 m $LiFeO_2$ (SEM shown, respectively, at ×265 or ×580 magnification). In the *top right panel* with 1 m $LiFeO_2$ (×265 magnification), and in the *bottom panel* with either 2 m (*left*), 3 m (*middle*), or 6 m (*right*) $LiFeO_2$. Electrolyses were conducted at 750 °C, rather than 730 °C, to improve dissolution of the concentrated Fe(III) electrolytes

Fig. 7. EDS of the black portions shows they are carbon, and the remainder iron. Hence, low Fe(III) concentrations provide a path to smaller STEP iron particles (albeit mixed with carbon). As seen in the other panels of Fig. 7, higher concentrations of $LiFeO_2$ (comparing 1, 2, 3 and 6 m concentrations) generate large iron metallic products. The iron electrolysis product particles are marginally larger at the highest (6 m) $LiFeO_2$ concentration (figure bottom right).

The cathode product is easily removed from wound steel wire cathode as it drops off upon uncoiling the wire. The fraction of trapped electrolyte retained in the cooled deposited STEP metal iron product is high. This electrolyte can be removed by washing and drying. The iron product is typically formed at high coulombic efficiency, and the iron metal formed is pure (not oxidized). However, the deposited iron resides with a large amount of electrolyte that is also extracted with the cathode. The percent by mass of iron metal in the product is 5–8 %, and the remainder is comprised of electrolyte. Extended charge electrolyses increase the percent by mass of iron metal in the product and decreases the amount of electrolyte contained with the product. Compared to the 1 Ah electrolysis in Fig. 2 (or the 0.2 or 2.5 Ah electrolysis in Fig. 6), Fig. 8 presents SEM of the iron product subsequent to a single 25 Ah electrolysis (1 A current (100 mA/cm^2) for 25 h). The percent of iron by mass in the product has increased to 11.5 %, and as seen, the iron particle size increases to ∼500 μm (ranging from 100 to 700 μm particle size).

Conclusions

Iron metal can be formed from iron oxide without the large carbon dioxide emissions that occur with the conventional industrial iron smelting, when the iron is formed by electrolysis in molten carbonate-containing dissolved Fe_2O_3 and Li_2O. In this study, we show that iron product micromorphology is substantially affected by the electrolysis conditions through the systematic variation of the electrolysis time, current density, temperature, and iron reactant and oxide concentrations. The iron product size decreases in size by a factor of 30 when the electrolysis current density is increased from 10 to 500 mA cm^{-2}.

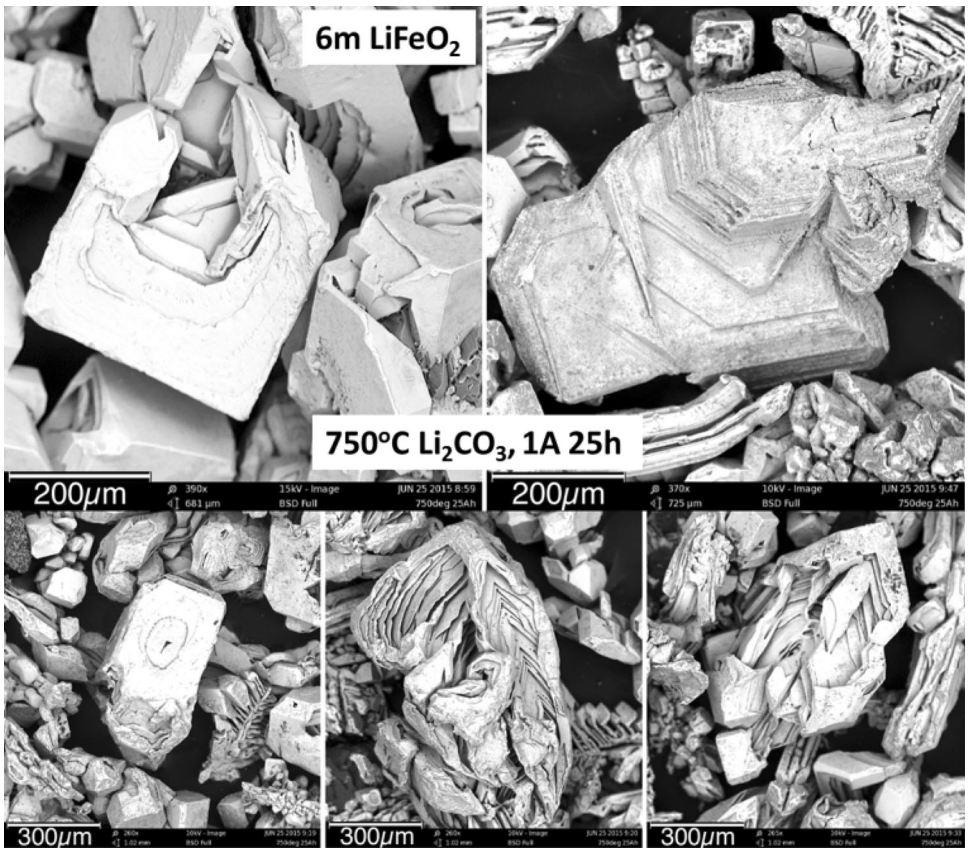

Fig. 8 Fe size subsequent to extended duration and charge electrolysis in Li_2CO_3 electrolytes. Variation of Fe iron formed in a single electrolysis at 1 A for 25 h (25 Ah of charge) at a 10 cm^2 iron cathode in 750 °C Li_2CO_3 containing 6 m $LiFeO_2$ (3 m Li_2O and 3 m Fe_2O_3)

Large (~500 μm) Fe is formed at low current densities during extended electrolysis, or at high Fe(III) concentrations. Small (~10 μm) Fe is formed at high current density and low concentration of Fe(III). The smallest particles generated are worthy of further study as catalysts, and were produced under conditions of the highest current and shortest electrolysis time. The iron product contains an observed magnetite overlayer when formed with hydroxide (LiOH) rather than oxide (Li_2O) added to the electrolyte. The observed deposited iron product particles are fiber shaped from equal molals of Li_2O and Fe_2O_3, but particle-like from electrolytes with surplus Li_2O. Iron is formed at high current efficiency, and the observed electrolysis potential decreases with (i) the decreasing current density, (ii) the addition of Li_2O, (iii) the increasing anode area, and (iv) the increasing temperature.

Acknowledgments This project was supported in part by a grant from the United States National Science Foundation 1230732.

References

1. Bloom B (2010) Iron, steel and cement production. The encyclopedia of earth. http://www.eoearth.org/view/article/161510/. Accessed 16 Dec 2010
2. Wang D, Gmitter AJ, Sadoway DR (2011) Production of oxygen gas and liquid metal by electrochemical decomposition of molten iron oxide. J Electrochem Soc 158:E51–E54
3. Kim H, Paramore J, Allanore A, Sadoway DR (2011) Electrolysis of molten iron oxide with an iridium anode: the role of electrolyte basicity. J Electrochem Soc 158:E101–E105
4. Allanore A, Yin L, Sadoway DR (2013) A new anode material for oxygen evolution in molten oxide electrolysis. Nature 497:353–356
5. Licht S, Wang B (2010) High solubility pathway for the carbon dioxide free production of iron. Chem Comm 47:7004–7006
6. Licht S, Wu H, Zhang Z, Ayub H (2011) Chemical mechanism of the high solubility pathway for the carbon dioxide free production of iron. Chem Comm 46:3081–3083
7. Cui B, Licht S (2013) Critical STEP advances for sustainable iron production. Green Chem 15:881–884
8. Licht S, Wu H (2011) STEP Iron, a Chemistry of iron formation without CO_2 emission: molten carbonate solubility and electrochemistry of iron ore impurities. J Phys Chem C 115:25138–25157
9. Ren J, Lau J, Lefler MJ, Licht S (2015) The minimum electrolytic energy needed to convert carbon dioxide to carbon by electrolysis in carbonate melts. J Phys Chem C 119:22342–22349
10. Licht S (2009) STEP (Solar Thermal Electrochemical Photo) generation of energetic molecules: a solar chemical process to

end anthropogenic global warming. J Phys Chem C 113:16283–16292
11. Licht S, Cui B, Wang B, Li F-F, Lau J, Liu S (2014) Ammonia synthesis by N_2 and steam electrolysis in molten hydroxide suspensions of nanoscale Fe_2O_3. Science 345:637–640
12. Licht S (2003) Solar water splitting to generate hydrogen fuel: photothermal electrochemical analysis. J Phys Chem B 107:4253–4260
13. Licht S, Halperin L, Kalina M, Zidman M, Halperin N (2003) Electrochemical potential tuned water splitting. Chem Comm 24:3006–3007
14. Licht S, Wang B, Ghosh S, Ayub H, Jiang D, Ganley J (2010) A new solar carbon capture process: solar thermal electrochemical photo (STEP) carbon capture. J Phys Chem Lett 1:2363–2368
15. Licht S (2011) Efficient solar-driven synthesis, carbon capture, and desalinization, STEP: solar thermal electrochemical production of fuels, metals, bleach. Adv Mater 47:5592–5612
16. Licht S, Wu H, Hettige C, Wang B, Asercion J, Lau J, Stuart J (2012) STEP cement: solar thermal electrochemical production of CaO without CO_2 emission. Chem Comm 48:6019–6021
17. Zhu Y, Wang H, Wang B, Liu X, Wu H, Licht S (2016) One-pot synthesis of carbon nanofibers from CO_2. Appl Cat B 193:151–159
18. Li F-F, Lau J, Licht S (2015) Sungas instead of syngas: efficient coproduction of CO and H_2 with a single beam of sunlight. Adv Science 1500260:1–5
19. Licht S, Cui B, Wang B (2013) STEP carbon capture: the barium advantage. J CO_2 Util 2:58–63
20. Li F-F, Liu S, Cui B, Lau J, Stuart J, Wang B, Licht S (2015) A one pot synthesis of hydrogen and carbon fuels from water and carbon dioxide. Adv Energy Mater 5:1401791-1-7
21. Gao GF, Li YC, Chen Y (2016) Dynamic response for porous epoxy resin matrix composites filled with iron powder at different strain rates and constitutive relationships. Mech Adv Mat Struct 23:811–868
22. Qing YC, Min DD, Zhou YY, Luo F, Zhou WC (2015) Graphene nanosheet- and flake carbonyl iron particle-filled epoxy-silicone composites as thin-thickness and wide-bandwidth microwave absorber. Carbon 86:98–107
23. Hola K, Markova Z, Zoppellaro G, Tucek J, Zboril R (2015) Tailored functionalization of iron oxide nanoparticles for MRI, drug delivery, magnetic separation and immobilization of biosubstances. Biotech Adv 33:1162–1176
24. Buceta B, Yoland P, Vázquez-Vázque C, Rivas J, López-Quintela M (2014) Metallic clusters: theoretical background, properties and synthesis in microemulsions. Catalysts 4:356–374
25. Gao F, Goodman DW (2012) Simulating the complexities of heterogeneous catalysts. Ann Rev Phys Chem 63:265–286
26. Li F-F, Licht S (2014) Advances in understanding the mechanism and improved stability of the synthesis of ammonia from air and water in hydroxide suspensions of nanoscale Fe_2O_3. Inorg Chem 53:10042–10044
27. Ren J, Li FF, Lau J, Gonzalez-Urbina Licht S (2015) One-pot synthesis of carbon nanofibers from CO_2. Nano Lett 15:6142–6148
28. Licht S, Douglas A, Ren J, Carter R, Lefler M, Pint CL (2016) Carbon nanotubes produced from ambient carbon dioxide for environmentally sustainable lithium-ion and sodium-ion battery anodes. ACS Cent Sci. doi:10.1021/acscentsci.5b00400